JGR Oceans

RESEARCH ARTICLE
10.1029/2019JC015019

Poleward Shift of the Pacific North Equatorial Current Bifurcation

Haihong Guo[1,2], **Zhaohui Chen**[1,2], **and Haiyuan Yang**[1,2]

[1]Physical Oceanography Laboratory/Institute for Advanced Ocean Study, Ocean University of China, Qingdao, China, [2]Pilot National Laboratory for Marine Science and Technology (Qingdao), Qingdao, China

Key Points:
- In the North Pacific, the North Equatorial Current bifurcation in the upper ocean shifts poleward with increasing depth
- The poleward shift of the bifurcation is associated with the asymmetric wind stress curl input to tropical/subtropical gyre
- The equatorial currents bifurcations in other basins share the same vertical structure

Correspondence to:
Z. Chen,
chenzhaohui@ouc.edu.cn

Citation:
Guo, H., Chen, Z., & Yang, H. (2019). Poleward shift of the Pacific North Equatorial Current bifurcation. *Journal of Geophysical Research: Oceans*, *124*. https://doi.org/10.1029/2019JC015019

Received 31 JAN 2019
Accepted 7 JUN 2019
Accepted article online 18 JUN 2019

Abstract The dynamics of the poleward shift of the Pacific North Equatorial Current bifurcation latitude (NBL) is studied using a 5.5-layer reduced gravity model. It is found that the poleward shift of the NBL is associated with the asymmetric intensity of the wind stress curl input to the Pacific tropical and subtropical gyres. Stronger wind stress curl in the subtropical gyre leads to equatorward transport in the interior upper ocean across the boundary between the two gyres, causing a poleward transport compensation at the western boundary. In the lower layer ocean, in turn, there is poleward (equatorward) transport at the interior (western boundary) due to Sverdrup balance which requires zero transport at the gyre boundary where zonally integrated wind stress curl is zero. Therefore, the NBL exhibits a titling feature, with its position being more equatorward in the upper layer and more poleward in the lower layer. The equatorial currents bifurcations in other basins are also characterized by the poleward titling vertical structure. The wind stress curl over the subtropical gyre is generally stronger than that over the tropical gyre, resulting in the bifurcations shifting poleward with increasing depth.

Plain Language Summary The bifurcation latitude of the North Equatorial Current bifurcation latitude (NBL) in the Pacific can be regarded as the boundary of the tropical and subtropical gyres. It also serves as the origin of the western boundary currents, the Kuroshio and the Mindanao Current, which are of great importance to mass and heat transport. Based on observations, it is found that the bifurcation shifts poleward with increasing depth in the upper ocean above the main thermocline. In this study, we show that the NBL tilting is induced by the asymmetric intensity of the wind stress curl input to the Pacific tropical and subtropical gyres. In a multilayered ocean model in which the wind stress curl over the subtropical gyre is stronger than that over the tropical gyre, there is anomalous equatorward (poleward) transport in the upper (lower) layer of the interior ocean. The anomalous interior transport requires poleward (equatorward) transport at the western boundary due to mass compensation, which is manifested as the bifurcation moves toward the tropical (subtropical) gyre in the upper (lower) layer ocean. Therefore, the NBL shifts poleward with increasing depth.

1. Introduction

The wind-driven components of the tropical Northwestern Pacific Ocean circulation system include the North Equatorial Current (NEC), the Kuroshio Current (KC), and the Mindanao Current (MC). Driven by the Pacific trade winds, the NEC is a quasi-steady westward current (Qu et al., 1998; Qu & Lukas, 2003; Toole et al., 1990), which bifurcates to form the southward flowing MC and the northward flowing KC as it encounters the Philippine coast (Nitani, 1972). It is believed that to some extent, the meridional movement of the NEC bifurcation latitude (NBL) determines the flow distribution of NEC, which has the potentials to play a vital role in local climate and western Pacific warm pool evolution (Kim et al., 2004; Qiu & Chen, 2010). In addition, the NBL also serves as the boundary between the Pacific subtropical gyre and tropical gyre, which is a good indicator of the meridional migration of the gyre-scale interactions (Qu, 2002).

The classic Sverdrup theory predicts that the Pacific NBL should lie at about 14.6 °N, where the basin-scale zonally integrated wind stress curl is generally zero (Sverdrup, 1947), and the theory is also true for the stratified ocean as we focus on the upper-layer ocean above the main thermocline (Welander, 1968). In the real ocean, however, the NBL is not vertically distributed, but characterized by the shift with increasing depth from 13.5 °N at the surface to farther north within and below the main thermocline (e.g., Qu, 2002; Qu et al., 1998; Qu & Lukas, 2003; Toole et al., 1990). Nitani (1972) first reported the

northward shift feature of the NBL, followed by more observational evidences based on geostrophic calculations using Levitus and World Ocean Atlas 2013 climatology (Locarnini et al., 2013; Zweng et al., 2013). In particular, Qu et al. (1998) showed that the NBL exhibits northward shift with increasing depth from about 13.5 °N at the surface to 18 °N at about 500 dbar. Subsequent studies suggested that the NBL occurs at about 14 °N near the surface, and it extends north of 20 °N in the upper intermediate layers (Qu, 2002; Qu & Lukas, 2003).

Except for observational approaches toward describing the northward shift of the NBL, this feature can be also captured by numerical models in recent works. Results from a high-resolution ocean general circulation model indicate that the NBL varies from 14.3 °N near the surface to 16.6 °N at around 500 m, which shows good agreement with previous hydrographic observations (Kim et al., 2004). A recent study by Jensen (2011) using a 4.5-layer reduced gravity model also found the poleward shift of the NBL given a stratification close to the observed, which means the poleward shift of the NBL from upper to lower ocean can be realistically reproduced in a simplified layered model.

With respect to the dynamical cause of this feature, Reid and Arthur (1975) attributed the vertical structure of the NBL to the poleward contraction of the subtropical gyre on denser waters. From the perspective of potential vorticity conservation, Toole et al. (1990) argued that the balance between changes in planetary vorticity and layer thickness should account for the NBL shift with increasing depth. In addition to the mean state, the vertical structure of the NBL also experiences significant seasonal variations (e.g., Chen & Wu, 2011; Kim et al., 2004; Qu & Lukas, 2003; Wang & Hu, 2006). Both observational and model results indicated the NBL moves equatorward with a weak poleward shift with depth in summer, while strong poleward shift occurs in winter (see Figures 11 and 14 of Qu & Lukas, 2003; Figure 4 of Kim et al., 2004). Although the vertical characteristic of the NBL as well as its seasonal variation was adequately revealed and simulated, the causes of these features are still not fully understood.

Motivated by the previous modelling work by Jensen (2011) who employed a purely wind-driven model and the success in reproducing the mean and seasonal cycle of the NEC bifurcation, we try to investigate the cause of the poleward shift of the NBL following his multilayer reduced gravity ocean model. This paper is organized as follows: Section 2 describes the data and model used in this study, followed by a series of box model experiments in section 3. In section 4, the causes of the NBL poleward shift are discussed in detail. The poleward shift of the bifurcations in global oceans will be discussed in section 5. Section 6 provides summary and further discussions.

2. Data and Model

2.1. Data

The World Ocean Atlas 2013 (Locarnini et al., 2013; Zweng et al., 2013) is used to construct the density field prescribed for the model. The Estimating the Circulation and Climate of the Ocean, Phase II (ECCO2, 1992–2016; Menemenlis et al., 2008) and the European Centre for Medium Range Forecast Ocean ReAnalysis Pilot 5 (ECMWF ORAP5, 1979–2013; Zuo et al., 2017) are used to calculate the NEC bifurcation off the Philippine coast. Both of these two data sets provide monthly zonal and meridional velocities with high spatial resolution (0.25° × 0.25°) to adequately depict the low-latitude western boundary currents. Considering the NEC mainly located in the upper ocean, we only use the upper 400-m velocities in these data sets. In addition, the climatological ECCO2 wind stress, the European Centre for Medium-Range Weather Forecasts (ECMWF) ERA-Interim reanalysis wind stress (1979–2017) with 0.25° × 0.25° resolution (Berrisford et al., 2009), the Florida State University (FSU) wind stress (1978–2003) with 1° × 1° resolution (Bourassa et al., 2005; Qiu & Lukas, 1996) and the climatological National Centers for Environmental Prediction (1° × 1° resolution; Kalnay et al., 1996) are used to force the models in this study.

In the western North Pacific near the Philippine coast, the NEC (Figure 1a), KC, and MC (Figure 1b) mainly concentrated upon the upper-layer ocean above the 12 °C isotherm that is conventionally used in previous studies (e.g., Qiu & Chen, 2012). The NBL in ECCO2 exhibits the northward shift with increasing depth from about 13 °N at the surface to 16 °N at about 400 m. The ECMWF ORAP5 shares the same vertical structure (not shown).

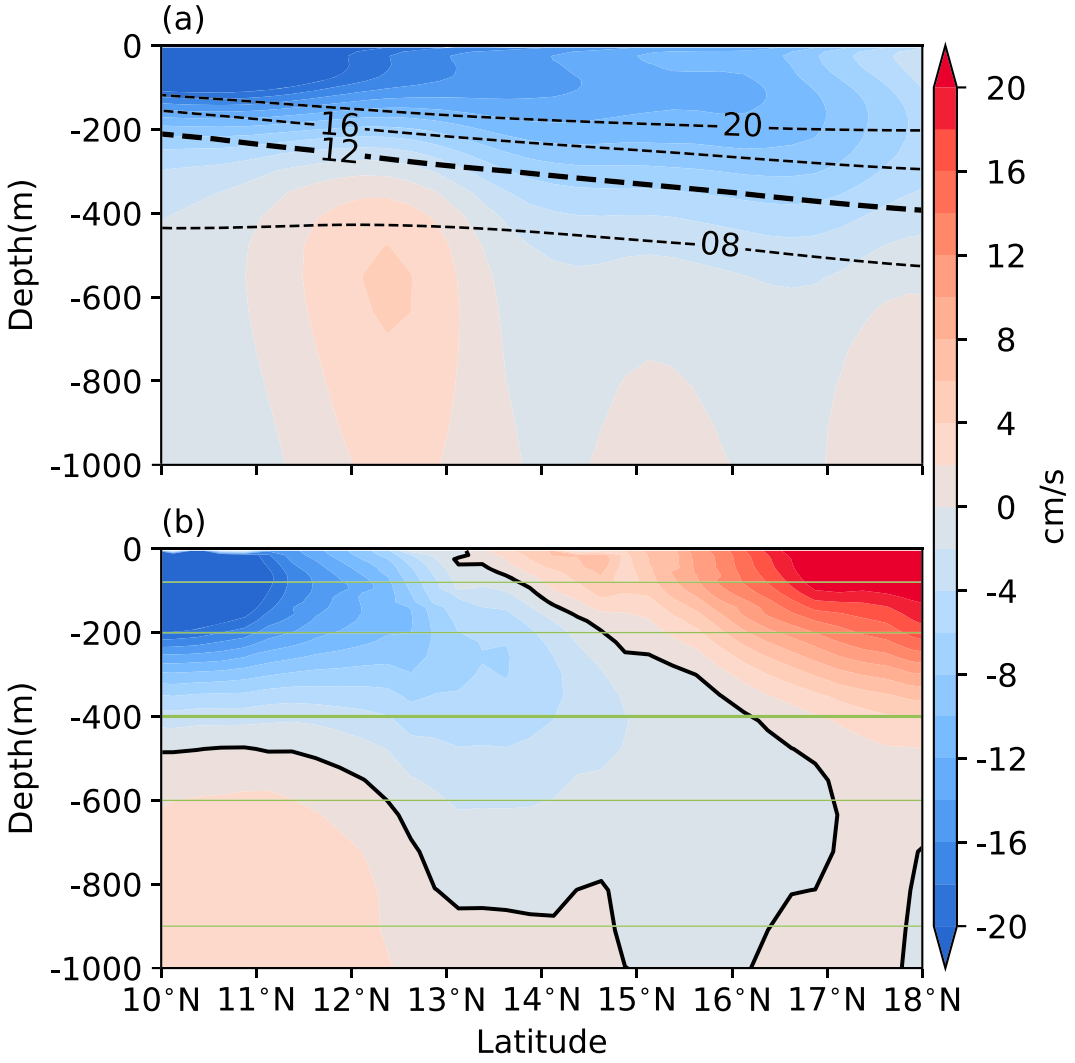

Figure 1. (a) Mean latitude-depth section of zonal velocity (color shading) and temperature (dashed lines) along 130 °E from ECCO2 (1992–2016). (b) Mean latitude-depth section of meridional velocity (color shading) averaged in the 2° longitude bands east of Philippine coast and solid black lines denote the zero velocity contours. The horizontal green line is the initial layers thickness of the reduced gravity model.

2.2. The Model

In this study, numerical experiments are performed using a 5.5-layer reduced gravity model based on the multilayer upper-ocean model developed by Jensen (1991, 1993). The governing equations for this model are as follows:

$$\frac{du_j}{dt} - fv_j = -\left(\sum_{i=j}^{5} g'_{i6}\frac{\partial h_i}{\partial x} + \left(1-\delta_{1,j}\right)\sum_{i=1}^{j-1} g'_{j6}\frac{\partial h_i}{\partial x}\right) + \frac{T_j^x}{\rho_0 h_j} + A_h\,\nabla^2 u_j + \left(1-\delta_{5,j}\right)\frac{W_j u_{j+1}}{H_{j+1}} - \left(1-\delta_{1,j}\right)\frac{W_{j-1}u_j}{H_j} \quad (1a)$$

$$\frac{dv_j}{dt} + fu_j = -\left(\sum_{i=j}^{5} g'_{i6}\frac{\partial h_i}{\partial y} + \left(1-\delta_{1,j}\right)\sum_{i=1}^{j-1} g'_{j6}\frac{\partial h_i}{\partial y}\right) + \frac{T_j^y}{\rho_0 h_j} + A_h\,\nabla^2 v_j + \left(1-\delta_{5,j}\right)\frac{W_j v_{j+1}}{H_{j+1}} - \left(1-\delta_{1,j}\right)\frac{W_{j-1}v_j}{H_j} \quad (1b)$$

$$\frac{\partial h_j}{\partial t} + \frac{\partial\left(h_j u_j\right)}{\partial x} + \frac{\partial\left(h_j v_j\right)}{\partial y} = \left(1-\delta_{5,j}\right)W_j - \left(1-\delta_{1,j}\right)W_{j-1} \quad (2)$$

where subscript j demotes layer number that changes from 1 to 5, u and v are the zonal and meridional

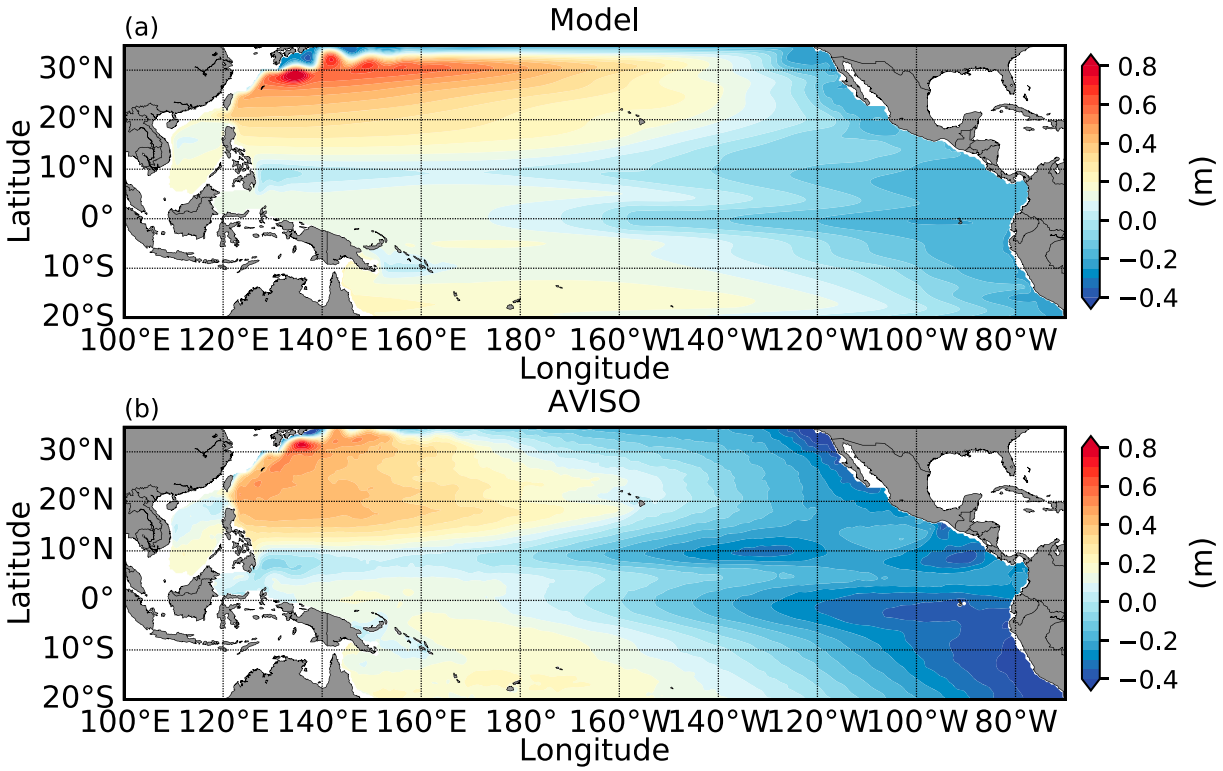

Figure 2. (a) Sea surface height anomaly displacement after 100 years spin-up driven by Florida State University wind stress. (b) Mean dynamic topography from AVISO surface. AVISO = Archiving, Validation, and Interpretation of Satellite Oceanographic.

velocities, h represents the perturbation of layer thickness of each layer, ρ_0 is the reference density, A_h is the lateral eddy viscosity, and $\delta_{i,j}$ is the delta function. The reduced gravity g' in each layer is defined as follows:

$$g'_{j6} = g\frac{\left(\rho_6 - \rho_j\right)}{\rho_0} \tag{3}$$

and T^x and T^y are the stresses between adjacent layers,

$$T^x_j = \delta_{1j}\tau^x_w + \left(1-\delta_{1j}\right)\tau^x_{j-1,j} - \left(1-\delta_{5j}\right)\tau^x_{j,j+1} \tag{4a}$$

$$T^y_j = \delta_{1j}\tau^y_w + \left(1-\delta_{1j}\right)\tau^y_{j-1,j} - \left(1-\delta_{5j}\right)\tau^y_{j,j+1} \tag{4b}$$

In equations (4a) and (4b), $\tau^x{}_w$ and $\tau^y{}_w$ are the zonal and meridional stresses that only act on the first layer, while $\tau^x_{j,j+1}$ and $\tau^y_{j,j+1}$ are the zonal and meridional frictions between layer j and layer $j+1$. To prevent the interface from surfacing, the entrainment and detrainment term W_j is adopted (see the Appendix A).

The governing equations are discretized onto C grid using second-order centered finite differences in space and Matsuno forward-backward scheme in time (Matsuno, 1966). The model domain covers the main part of the Pacific Ocean (100 °E–70 °W, 20 °S–35 °N) with horizontal resolution of 0.25°. Marginal seas shallower than 600 m are treated as land, and all the islands in the interior of ocean are neglected. The initial layer thicknesses of the five active layers are 80, 120, 200, 200, and 300 m, which are consistent with previous model studies (Jensen, 2011; Qu et al., 1998). Based on the density derived from WOA 2013 in the NEC bifurcation region, we obtained the density stratification whose sigma-theta levels are constant in each isopycnal layer. Here the sigma-theta levels are chosen to be 23.9, 25.5, 26.5, 26.9, 27.2, and 27.7, respectively. To maintain a realistic layer thickness in each layer, we set the minimum layer thickness 40, 60, 100, 100, and 150 m and the maximum layer thickness 120, 180, 300, 300, and 450 m. As mentioned above, there will be entrainment (detrainment) if the layer thickness is thinner (thicker) than the prescribed minimum (maximum) thickness. No normal flow and no-slip boundary conditions are employed along the lateral boundary.

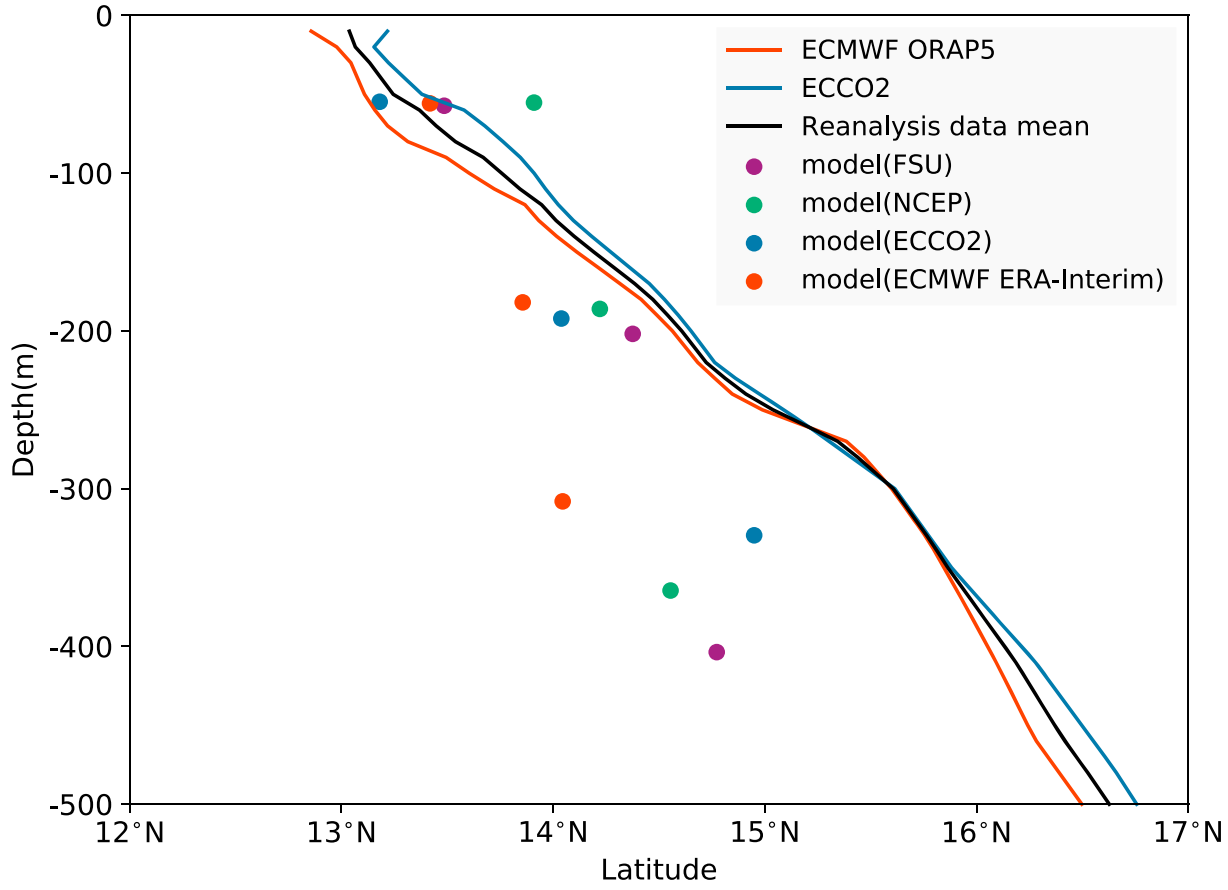

Figure 3. Vertical distribution of North Equatorial Current bifurcation latitude in different assimilation data (color lines), mean of all data mentioned above (black line). Modeled North Equatorial Current bifurcation latitude position in each layer driven by FSU (purple dot), NCEP (green dot), ECCO2 (blue dot) and ECMWF ERA-Interim (red dot). ECMWF ORAP5 = European Centre for Medium Range Forecast Ocean ReAnalysis Pilot 5; ECCO2 = Estimating the Circulation and Climate of the Ocean, Phase II; FSU = Florida State University; NCEP = National Centers for Environmental Prediction.

2.3. Model Performance

Before calculating the modelled bifurcation that is confined to the western boundary, it is beneficial to first examine the capability of simulating the broad scale circulation using this multilayer model. Here we derived the baroclinic sea surface height η from model output, which is defined as (Jensen, 2011)

$$\eta = \sum_{i=1}^{5} \frac{\rho_6 - \rho_i}{\rho_6} (H_i - H_{0i}) \tag{5}$$

where H_i is the layer thickness and H_{0i} is the initial layer thickness at rest (e.g., Jensen, 2001, 2003, 2011). It is shown in Figure 2 that the sea surface height anomaly resembles the pattern observed by the Archiving, Validation, and Interpretation of Satellite Oceanographic mean dynamic topography (Rio et al., 2011), implying that the layered reduced model is capable of reproducing the overall pattern of the tropical and subtropical gyre in the North Pacific as well as the low-latitude western boundary current system.

Figure 1 has shown that the NEC, KC, and MC mainly focus on the upper three layers covering the upper 400 m. Figure 3 shows the modeled NBL in the upper three layers and the vertical structure of the NBL obtained from two reanalysis/assimilation data sets (ECCO2 and ECMWF ORAP5). The bifurcation latitude is conventionally defined as the latitudinal position where the averaged meridional flow within 2° band off the Philippine coast is zero. It is shown that the bifurcation generally shifts toward the north with increasing depth from 13 °N near the surface to 16 °N at 400 m, which is close to reanalysis/assimilation data sets and previous studies (Kim et al., 2004; Qu, 2002; Qu & Lukas, 2003). Compared to the reanalysis/assimilation results, the modelled poleward tilt of the NBL in upper three layers is relatively weak, which may be

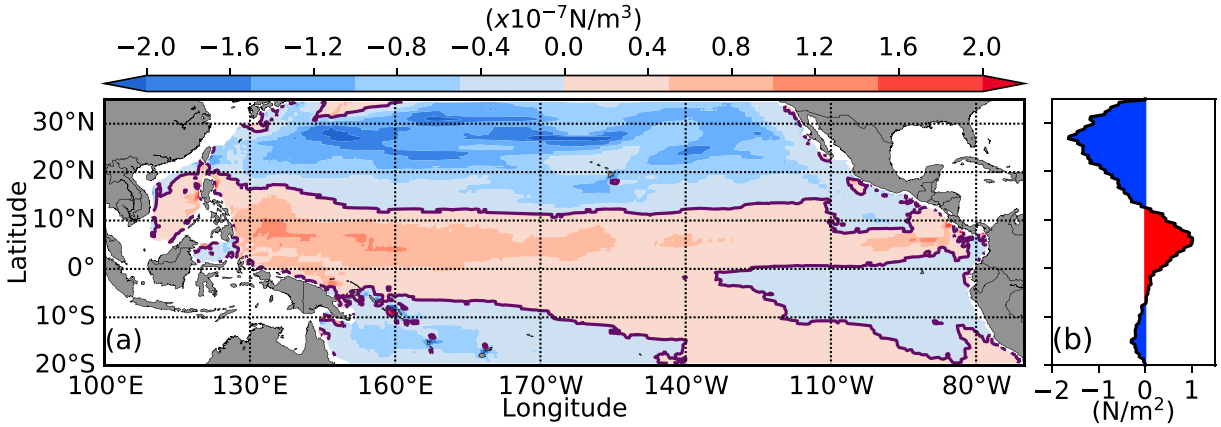

Figure 4. (a) Wind stress curl of FSU wind stress (color shading) and zero line of wind stress curl (solid lines). (b) Zonally integrated wind stress curl as a function of latitude.

attributed to the absence of thermo-dynamics in the model. Even though the discrepancy between model results and reanalysis/assimilation products is significant, it will not pose a serious problem in depicting the overall pattern of its vertical feature. In general, the vertical structure of the NBL can be adequately simulated in 5.5-layer reduced gravity model.

3. Box Model Experiments

It has demonstrated in section 2 that the 5.5-layer reduced gravity model can well simulate the basin-scale circulation and the NEC bifurcation. Since the coastline shape plays a minor role in regulating the NBL (Jensen, 2011), it is straightforward to employ a simplified box model to explore the dynamical mechanism of NBL poleward shift.

The east-west span of the box model is 120°, which is close to the basin width of the low-latitude Pacific Ocean. The south-north span of the box model is 30°, representing the meridional span 0-30 °N. For simplicity, the β-plane approximation is adopted, with the reference latitude being 15 °N. In the box model, we only apply the wind stress in zonal direction. In addition, the wind stress and wind stress curl are set zonally uniform considering the quasi-zonal structure of wind stress in the North Pacific (Figure 4a). It is also shown in Figure 4b that the zonally averaged wind stress curl over the subtropical gyre is stronger than that over the tropical gyre, and we presume that the different intensity of the wind stress forcing should account for the poleward shift of the NBL. As will be shown latter, the asymmetry of the wind field is key to determine the NBL vertical structure. Other model parameters are same with the model in section 2.

To test the potential role of asymmetric wind forcing in determining the vertical titling of NBL, we designed three parallel experiments: EXP-A, EXP-B, and EXP-C. The wind stress curl in the subtropical gyre is set to be the same in three experiments, whereas the amplitude of wind stress curl in the tropical gyre is set to be as same, half, and twice as that in the subtropical gyre in EXP-A, EXP-B, and EXP-C, respectively (equation (6) and Figure 5), where y is latitude, $A = 0.015$ is the amplitude of the wind stress in equation (6).

$$\tau_w^x = \begin{cases} A\times\cos\left(\frac{\pi}{15}\times y\right), & (y = 0\sim 15°N) \quad \text{EXP-A} \\ \frac{A}{2}\times\cos\left(\frac{\pi}{15}\times y\right) - \frac{A}{2}, & (y = 0\sim 15°N) \quad \text{EXP-B} \\ 2A\times\cos\left(\frac{\pi}{15}\times y\right) + A, & (y = 0\sim 15°N) \quad \text{EXP-C} \\ A\times\cos\left(\frac{\pi}{15}\times y\right), & (y = 15°N\sim 30°N) \end{cases} \tag{6}$$

It is shown in Figure 5a3 that the modelled NBL is vertically uniform, basically coincided with 15 °N where the zero line of wind stress curl locates. Compared to EXP-A, the vertical structure of the modelled NBL in

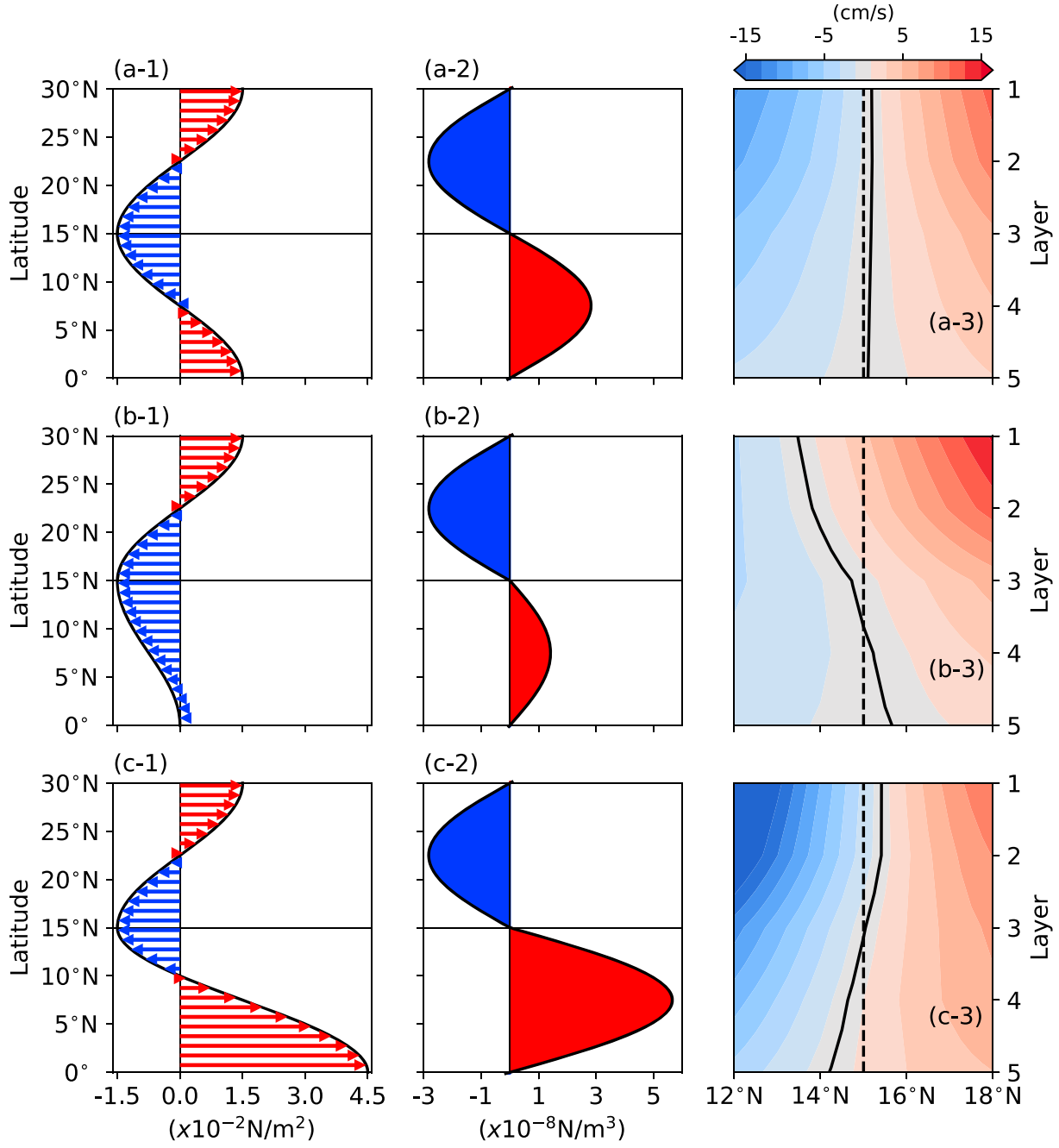

Figure 5. Meridional distribution of (a-1) zonal wind stress and (a-2) wind stress curl in EXP-A. (b-1 and c-1) and (b-2 and c-2), same as (a-1) and (a-2) but for zonal wind stress and wind stress curl in EXP-B and EXP-C. (a-3) Meridional velocity averaged in the 2° longitude bands (color shading) derived from EXP-A, the solid line indicates the bifurcation, and the dashed line denotes the gyre boundary (15 °N). (b-3 and c-3) Same as (a-3) but for results in EXP-B and EXP-C.

the following two experiments are characterized by opposite tilting with increasing depth. In EXP-B (Figure 5b3), the NEC bifurcates at 13.8 °N in the first layer (50 m) and 15.6 °N in the deepest layer (750 m), which is identical to the realistic model run (Figure 3). Conversely, the bifurcation in EXP-C (Figure 5c3) locates at 15.5 °N in the first layer (40 m) and shifts to 14.2 °N in the deepest layer (770 m). The different vertical structures of the NBL in three experiments imply a potential role of relative magnitude of wind stress curl over subtropical/tropical gyres. In other words, the poleward (equatorward) shift of NBL with increasing depth corresponds to the relatively stronger (weaker) intensity of wind stress

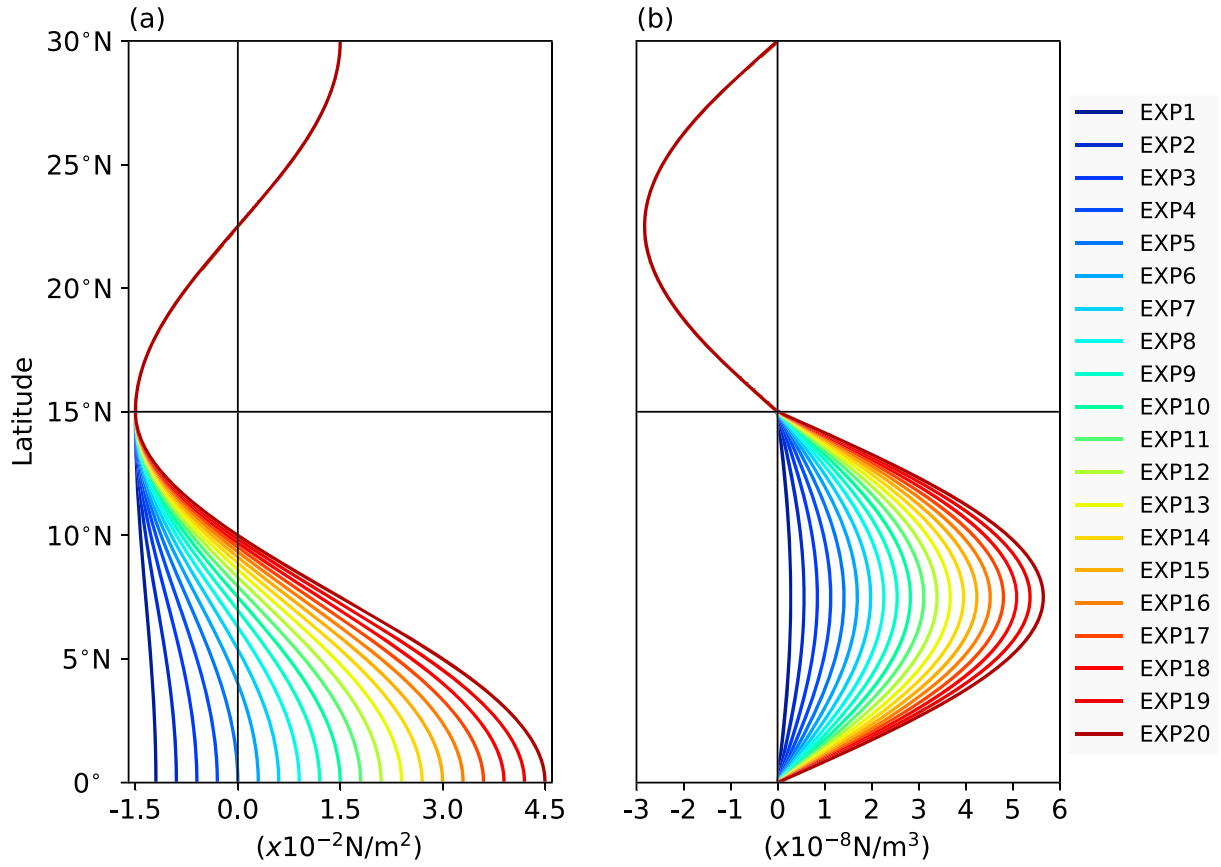

Figure 6. (a) Zonal wind stress and (b) wind stress curl in EXP 1 to 20.

curl over the subtropical (tropical) gyre (Figure 5). In the following part, we will test this relationship by successively changing the relative magnitude of wind stress curl over the two gyres.

Consistent with the wind forcing in EXP-B and EXP-C, the intensity of the wind stress over the tropical gyre is artificially set in the following sensitivity experiments (Figure 6), so that the wind stress curl over the tropical gyre increases gradually from 10% to 200% of that over the subtropical gyre. Like the realistic model run in last section, all these experiments are spun-up for 100 years spin-up to reach the steady state.

$$\tau_w^x = \begin{cases} \frac{i}{10}\times A\times\cos\left(\frac{\pi}{15}\times y\right) + \frac{i-10}{10}\times A, & (y = 0^{\sim}15^{\circ}N) \\ A\times\cos\left(\frac{\pi}{15}\times y\right), & (y = 15^{\circ}N^{\sim}30^{\circ}N) \end{cases} \tag{7}$$

where y and A are the same as that in equation (6). The subscript i denotes the ith run from EXP 1 to EXP 20 (Figure 6).

To better illustrate the relationship between the wind forcing and the NBL vertical tilting, we define the asymmetry index for mean circulation and wind forcing as follows:

$$\delta_\psi = (\max(|\psi_{TG}|) - \max(|\psi_{SG}|))/\max(|\psi_{SG}|) \tag{8}$$

$$\delta_{curl} = \left(\left|\iint_{TG}\mathrm{curl}\right| - \left|\iint_{SG}\mathrm{curl}\right|\right)/\left|\iint_{SG}\mathrm{curl}\right| \tag{9}$$

where the subscript SG and TG denote the subtropical gyre and tropical gyre, respectively. According to equations (8) and (9), δ_ψ describes the relative intensity of the streamfunction between the tropical and subtropical gyre (Chang et al., 2001; Sun et al., 2013), which characterize the gyre-scale asymmetry of the mean

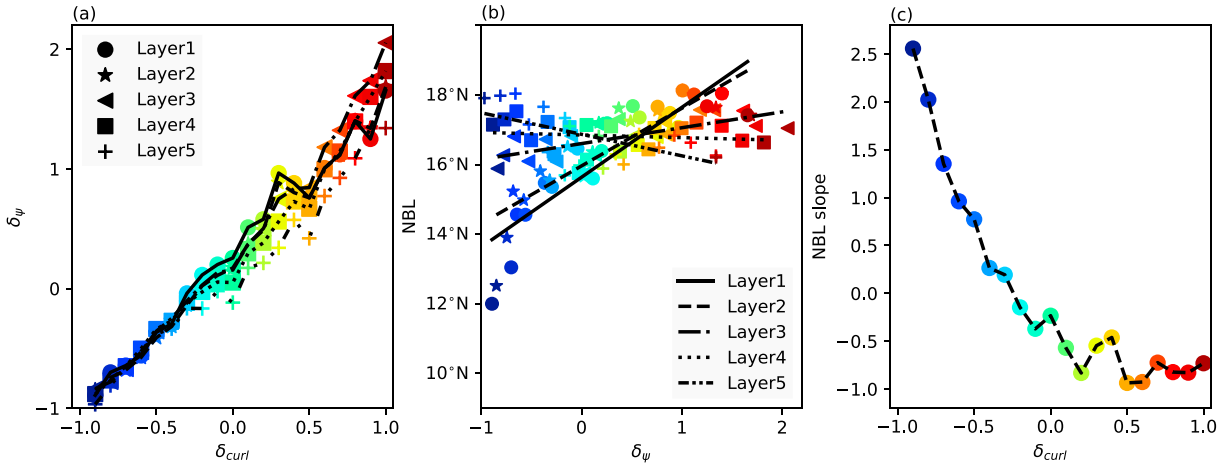

Figure 7. (a) Scatterplot of the wind stress curl difference in terms of δ_{curl} and modeled gyre-scale circulation difference in terms of δ_ψ. (b) Same as (a) but for the modeled NBL and δ_ψ. The dashed lines are linear fittings. (c) The normalized NBL slope as a function of δ_{curl}. The colors represent experiments from 1 to 20 as shown in Figure 6. NBL = North Equatorial Current bifurcation latitude.

circulation. Similarly, we also define δ_{curl} as the relative intensity of the wind stress curl between the tropical and subtropical gyre. If δ_ψ equals to zero, the intensity of circulation in the subtropical is the same as that in the tropical gyre. With the increasing of δ_ψ, the circulation of two gyres becomes more asymmetric (Figure 7a). In particular, a stronger wind stress curl over the subtropical gyre leads to a more enhanced western boundary current of the subtropical gyre (e.g., Kuroshio in the North Pacific or East Australian Current in the South Pacific). This relationship between wind and circulation holds for all five layers in the sensitivity experiments.

We also compared the evolution of the NBL versus δ_ψ in each layer in Figure 7b. It is found that the linear correlation between the NBL migration and circulation asymmetry is positive in upper three layers, indicating a significant positive relationship between the tropical circulation intensity and northward migration of the bifurcation. However, the NBL migration in the lower two layers exhibits an opposite relationship but is not as prominent as the upper layers.

We further calculated the tilt of the bifurcation in terms of latitude deviation. It is demonstrated that the shift of the NBL is generally determined by the relative intensity of wind stress curl over the two gyres (Figure 7c). In other words, strong poleward shift of the NBL with increasing depth is always accompanied by relatively strong wind stress curl input to the subtropical gyre. Next, we will explain the controlling dynamics behind this phenomenon.

4. Cause of Poleward Shift of Modeled NBL

As revealed in the last section, the NBL vertical distribution shows a remarkable relationship between the wind stress curl and mean circulation in the western boundary (recall Figures 5 and 7). Sverdrup theory indicates that the strength of western boundary current is compensated by total meridional transport in the interior ocean, which is determined by the wind stress curl across the entire basin.

With symmetric wind stress curl in the tropical and subtropical gyre, the NBL shows vertically uniform distribution (EXP-A), and the meridional transport across the gyre boundary is close to zero. Taking the symmetric experiment (EXP-A) as the reference experiment, we calculated the anomalous transports of EXP-B/C at 15 °N (Table 1). In the upper layers, particularly for layers 1 and 2, there is a prominent anomalous southward (northward) transport in EXP-B (EXP-C) in the interior ocean, while the lower layers show opposite anomaly in the two experiments. This feature is somewhat analogous to those proposed by a recent study by Yang (2015).

Table 1
The Anomalous Meridional Transports (Sv.) in Each Layer Calculated in Ocean Interior at 15 °N and the Mean Transport of EXP-A Has Been Subtracted

	Layer 1	Layer 2	Layer 3	Layer 4	Layer 5
EXP-B	−2.03	−0.96	0.09	0.37	0.53
EXP-C	0.86	1.77	−1.07	−1.23	−1.49

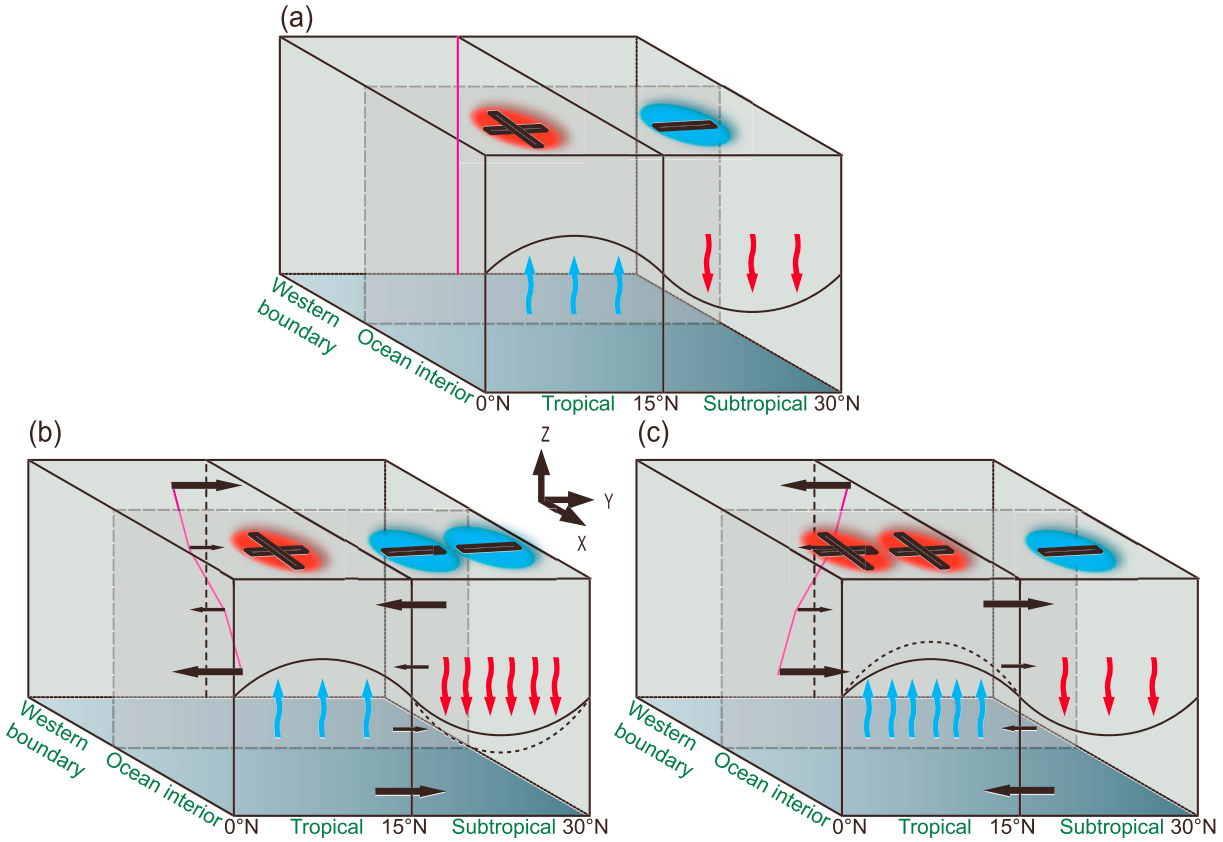

Figure 8. The schematics of the response of interior/western boundary transport to wind stress curl asymmetry in (a) EXP-A, (b) EXP-B, and (c) EXP-C. The circles denote wind stress curl, the black arrows are anomalous transports across 15 °N, and the pink lines represent the North Equatorial Current bifurcation latitude.

With respect to the western boundary, as we can see from Figure 5b3, there is northward (southward) transport anomaly across 15 °N in upper (lower) layers, which compensate the interior flow due to mass conservation. The NBL in the upper (lower) layers, therefore, shift southward (northward) in EXP-B and vice versa for EXP-C.

The anomalous meridional transport in each layer readily links the western boundary current transport anomaly with different scenario of wind stress forcing over two gyres. We show in Figure 8 the schematic for the dynamic mechanism of the vertical structure of NBL. When the wind stress curl over the subtropical gyre is stronger than that over the tropical gyre, there is anomalous southward (northward) transport in the upper (lower) interior ocean, resulting in anomalous northward (southward) transport at the upper (lower) western boundary. In this sense, the anomalous western boundary currents are manifested as equatorward (poleward) migration of the NBL in the upper (lower) layer, showing the poleward shift of NBL with increasing depth (Figure 8b). This explanation also holds for the case when the wind stress curl is stronger in the tropical gyre (Figure 8c).

The relationship between the NBL shift and wind forcing can be revealed in terms of energy balance as well. Diagnosing the outputs from previous 20 sensitivity runs, we found in Figure 9a that there is strong relationship between wind stress curl asymmetry (δ_{curl}) and asymmetric energy input to respective gyres (δ_E; see Appendix B for more details). Further examination of energy budget suggests that for the steady state of the ocean circulation, the energy input from the wind is balanced by lateral dissipation.

Although the total energy is conserved over the whole basin, the spatial distribution of lateral dissipation is uneven. We then calculated the accumulated lateral dissipation from the western to eastern boundary, and it is shown in Figure 9b that the dissipation within the western boundary accounts for about 90% of the total energy dissipation. In this regard, it is reasonable to relate the lateral dissipation intensity along the western boundary with the energy input from the wind. For the cases above, a strong gyre-scale circulation requires

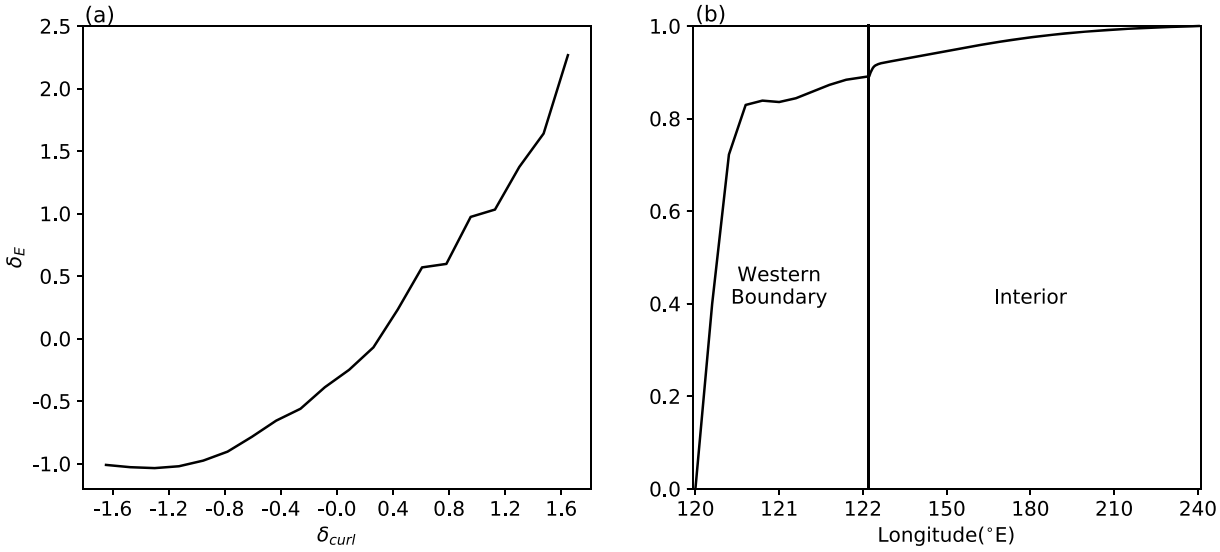

Figure 9. (a) Relationship between normalized wind stress curl difference in terms of δ_{curl} and gyre-scale energy input δ_E. (b) Normalized meridional lateral dissipation integrated from the western boundary to each longitude, and the results are averaged from the 20 experiments.

an elongated western boundary current for sufficient dissipations, which is manifested as western boundary current intrusions to the other gyre. Therefore, the bifurcation latitude in the upper layer shifts to the weaker side of the gyre rather than locating at the zero line of zonally integrated wind stress curl.

5. Bifurcations in Global Oceans

The NEC and South Equatorial Current (SEC) bifurcations are universal in low-latitude oceans and their vertical structures share the same feature, i.e., poleward titling bifurcation with increasing depth (Figure 10). In the southern hemisphere, for example, the Atlantic South Equatorial Current (ASEC) bifurcates into the North Brazil Undercurrent to the north and Brazil Current to the north. Observations and modelling studies suggest that the ASEC bifurcation occurs 10–14 °S near the surface, shifts poleward with increasing depth, and reaches 27 °S at 1,000 m (Rodrigues et al., 2007). Compare to the large south-north extent of the bifurcation, the Indian South Equatorial Current (ISEC) bifurcation off the Madagascar coast shifts from 17.5 °S at the surface to 19 °S at 400 m, with its depth mean position at 18.1 °S (Chen et al., 2014). As a counterpart of the NEC bifurcation in the North Pacific, the Pacific South Equatorial Current (PSEC) bifurcation locates just north of 16 °S at the surface and near 22 °S at 800 m (Chen & Wu, 2015; McCreary et al., 2007).

Since all of these bifurcations are characterized by poleward shift with increasing depth, it is helpful to further examine the wind stress curl over two gyres of each basin. It is shown in Figure 10 that the intensity of wind stress curl on both sides of zero curl lines are asymmetrically distributed, where wind stress curl over the subtropical gyre is much stronger than the tropical gyre. We also highlight the intensity difference of wind stress curl between two gyres in determining the degree of tilting. Here we define the wind stress curl ratio (r_{curl}) as the ratio of wind stress curl intensity of the subtropical gyre to the tropical gyre. In the same way, we calculated the bifurcation latitude slope (s) to demonstrate the degree of tilting. In ECCO2, the strongest asymmetric wind stress curl occurs in South Atlantic with a ratio of 6.69, and its bifurcation latitude slope is the most prominent as well (34×10^{-3} °/m). In the Pacific basins, the wind stress curl ratio in the North (South) Pacific is 2.85 (2.97) with the bifurcation slope 7.3×10^{-3} °/m (9.0×10^{-3} °/m). For the bifurcation in the Indian Ocean where SEC splits off the Madagascar coast, the slope is only 5.3×10^{-3} °/m which is probably due to the small ratio (2.74; Table 2). The overall results are basically in accord with our findings that the wind stress curl ratio determines the level of bifurcation shift. The relationship between wind forcing and bifurcation tilting can be also found in ECMWF-ORAP5.

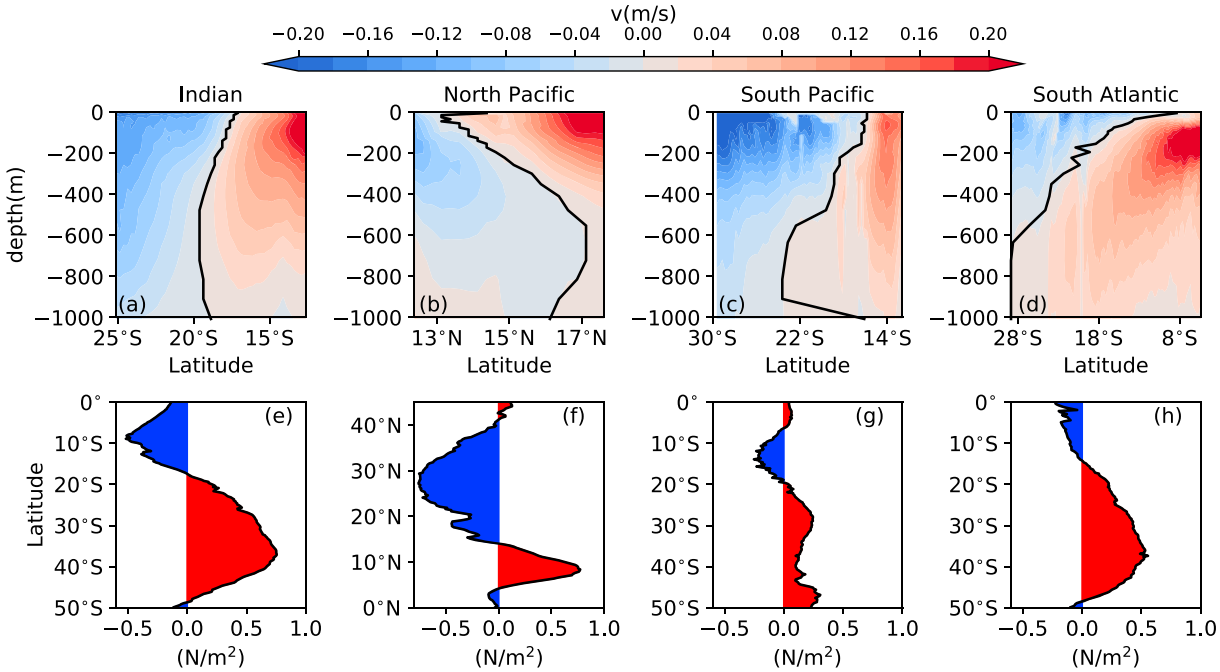

Figure 10. (a) Mean latitude-depth section of meridional velocity (color shading) averaged in the 2° longitude bands east of Madagascar coast and solid black lines denote the zero velocity contours. (e) Zonally integrated wind stress curl over the Indian Ocean as a function of latitude. (b–d) Same as (a) but for the North Pacific, South Pacific, and South Atlantic. (f–h) Same as (e) but for the North Pacific, South Pacific, and South Atlantic.

6. Summary and Discussions

In this study, we have investigated the vertical structure of the NEC bifurcation off the Philippine coast. The NEC bifurcation exhibits a poleward tilting with increasing depth, and it shifts from 13.1 °N at surface to 16.4 °N at 500 m. Model experiments using a 5.5-layer, nonlinear, reduced gravity, primitive equation model suggest that the poleward shift of the NEC bifurcation is associated with the asymmetric intensity of wind forcing over the subtropical and tropical gyre.

We found in this study that the wind stress curl asymmetry is of great importance in determining the NBL poleward tilting. If the two gyres are forced by the wind stress curl with comparable intensity, the bifurcation in the model will be independent of layers. If the wind stress curl over the two gyres is significantly asymmetrically distributed, there will be an anomalous transport to the weak side of gyre in the upper layers. To compensate the anomalous transport in ocean interior, there is an opposite transport anomaly at the western boundary. Therefore, the modelled bifurcation in the upper layers would shift toward the weaker side of gyre, and the NBL will be characterized by the poleward shift feature.

In terms of energy balance, we found that the energy input from the wind is mainly balanced by the lateral dissipation at the western boundary. In the upper layers, a stronger gyre needs more lateral dissipation to balance the energy input from the winds, so that the bifurcation latitude shifts to the weaker side to elongate the flow path of the western boundary current.

Table 2
The Wind Stress Curl Intensity Ratio and the Bifurcation Slope

	ECCO2		ECMWF ORAP5	
	r_{curl}	s ($\times 10^{-3}$°/m)	r_{curl}	s ($\times 10^{-3}$°/m)
NP	2.85	7.3	2.82	8.5
SA	6.69	34	5.90	30
SI	2.74	5.3	2.70	7.3
SP	2.97	9.0	2.95	9.1

Note. Table 2 contains wind stress curl intensity ratio and bifurcation slope of North Pacific (NP), South Atlantic (SA), South Indian Ocean (SI), and South Pacific (SP) in ECCO2 and ECMWF ORAP5.

The above box experiments are all based on a constant β value (β plane with reference value being fixed at 15 °N), which means the interior Sverdrup transport is linearly correlated with the wind stress curl. For nonconstant β value, we have conducted an additional experiment forced by symmetric wind with real β value and found that the NBL has a slight tilting (not shown). This can be easily understood that β decreases toward the pole, and the interior transport response to wind forcing is slightly different. In other words, the variation of β value imposes nonnegligible impact on the NBL

vertical distribution structure; nevertheless, it is still incomparable to the asymmetric external wind forcing.

The poleward shift of the bifurcation as well as the upstream equatorial currents can also be understood in terms of beta spiral theory (Stommel & Schott, 1977). In the subtropical North Pacific, the Ekman flux has a nonzero divergence that pushes a downward motion in the subtropical basin, which leads to a right-hand spiral structure. Since the westward NEC is the boundary between subtropical gyre and tropical gyre, there should be a right-hand spiral with increasing depth. The spiral results in the poleward contraction of subtropical gyre over denser water (Reid & Arthur, 1975), which is manifested as the poleward shift of bifurcation latitude (gyre boundary) with increasing depth. However, this argument seems valid only for the interior ocean, and its validations at the western boundary need further discussions.

Another issue we should address here is the modelled undercurrents. For example, the Luzon Undercurrent (LUC) and Mindanao Undercurrent (MUC) are import components of the equatorial currents in the Northwestern Tropical Pacific Ocean, and they have been shown to be dynamically important to the three-dimensional circulations (Hu et al., 2013; Hu & Cui, 1989). In the last two decades, there are plenty of researches focusing on the dynamic mechanism of their origins (Chiang & Qu, 2013; Wang & Hu, 2012; Zhang et al., 2014). Although we have successfully reproduced the KC and MC and associated NBL in our multilayered model, the currents like LUC and MUC beneath them are not adequately captured. The model is highly simplified and lacks of sufficient physical processes, so we believe that the undercurrents cannot be modelled. But it would be interesting for future researches to investigate the LUC and MUC by adding more physical processes in our model.

There are many factors that account for the poleward shifting of the bifurcation. We admit that it is not sufficient to get a full picture of the bifurcation from the purely wind-driven layered model with other processes like buoyancy forcing absent in the model. What's more, we only focused on the time-averaged structure of the circulation and the associated bifurcation in this study, and we have not discussed the temporal variations of the bifurcation and its vertical structure. This issue will be addressed in the following study, in particular, the adjustment processes need to be clarified in detail.

Appendix A: Entrainment and Detrainment Terms in the Model

The term W_j in equations (1a) and (1b) denotes the entrainment and detrainment between layer j and layer $j + 1$.

$$W_j = w_{ej,j+1} + w_{dj,j+1} \tag{A1}$$

$$w_{ej,j+1} = \begin{cases} \dfrac{(H_e - h_j)^2}{t_e H_e}, h_j < H_e \\ 0 \qquad\qquad\qquad , h_j \geq H_e \end{cases} \tag{A2}$$

In equation (A2), $w_{ej,\,j+1}$ is defined as the entrainment in the model (McCreary & Kundu, 1988, 1989), which makes good physical sense and prevents the interface from surfacing. It should be noted that the entrainment only occurs when $h_j < H_e$, where H_e is a minimum value that was prescribed in each layer. As long as $h_j < H_e$, w_e will increase parabolically toward a maximum value of H_e/t_e, where t_e is the entrainment time scale to ensure that the interface between layers dose not surface (McCreary & Kundu, 1988). The converse is seen when the layer thickness becoming larger than H_d, a detrainment constraint is also applied that is expressed the same as the entrainment term (Jensen, 2001)

$$w_{dj,j+1} = \begin{cases} -\dfrac{(h_j - H_d)^2}{t_d H_d}, h_j > H_d \\ 0 \qquad\qquad\qquad , h_j \leq H_d \end{cases} \tag{A3}$$

According to equation (A3), the detrainment only exists when $h_j > H_d$. It is found that the entrainment and detrainment terms are necessary conditions for model stability through a series of model tests and they will not be addressed in present study.

Appendix B: Energy Equation

We define the asymmetry of energy input to respective gyres as follows:

$$\delta_E = \left(\iint_{TG} E - \iint_{SG} E\right) / \iint_{SG} E \tag{B1}$$

The correlation coefficients between δ_{curl} and δ_E is 0.94. The kinetic energy (KE) in the model is as follows:

$$KE_j = \frac{1}{2}\left(u_j^2 + v_j^2\right) \tag{B2}$$

where (u_j, v_j) is the velocity vector of layer j. Using momentum equations in equations (1a) and (1b), we can derive the kinetic energy equation as follows:

$$\begin{aligned}\frac{dKE_j}{\partial t} = &-\left(\sum_{i=j}^{5} g'_{i6}\left(u_j\frac{\partial h_i}{\partial x} + v_j\frac{\partial h_i}{\partial y}\right) + \left(1-\delta_{1,j}\right)\sum_{i=1}^{j-1} g'_{j6}\left(u_j\frac{\partial h_i}{\partial x} + v_j\frac{\partial h_i}{\partial y}\right)\right) + \frac{\mathbf{v}_j \cdot T_j}{\rho_0 h_j} \\ &+A_h \mathbf{v}_j \nabla^2 \mathbf{v}_j + \left(1-\delta_{5,j}\right)\frac{W_j\left(u_j u_{j+1} + v_j v_{j+1}\right)}{H_{j+1}} - \left(1-\delta_{1,j}\right)\frac{W_{j-1}\left(u_j^2 + v_j^2\right)}{H_j}\end{aligned} \tag{B3}$$

According to equation (B3), the local change of KE is balanced by advection, pressure gradient, external wind forcing, lateral dissipations, and energy exchange caused by W_j between adjacent layers. Diagnoses of energy budget suggest that the KE advection and pressure gradient are conserved if we integrate over the entire basin. In addition, the energy exchanges between adjacent layers are weak.

We derived the position of minimum lateral dissipation to explore the mechanisms responsible for the vertical distribution of the NBL. Not surprisingly, the minimum lateral dissipation position in each layer agrees well with the modeled NBL. The correspondence between them is easy to be understood because the lateral dissipation is mainly determined by $A_H v_{xxx}$, which means it must follow the shift of the bifurcation that requires the minimum meridional velocity.

Acknowledgments

This research is supported by National Natural Science Foundation of China (41622602, 41806008, and U1606402) and Pilot National Laboratory for Marine Science and Technology, Qingdao, (2017ASTCPES05 and 2017ASKJ01). Z. C. is partially supported by the "Taishan" Talents program, and H. Y. is partially supported by the Chinese Scholarship Council. The WOA13, ECCO2, ECMWF ORAP5, FSU, NCEP, and AVISO products used this study can be obtained through the URLs: http://www.nodc.noaa.gov/, http://ecco2.org, http://www.myocean.eu/web/69-myocean-interactive-catalogue.php?option=com_csw&view=details&product_id=GLOBAL_REANALYSIS_PHYS_001_017, https://www.coaps.fsu.edu/RVSMDC/FSUFluxes/index.php, http://apdrc.soest.hawaii.edu/data/2, and http://www.aviso.oceanobs.com/, respectively.

References

Berrisford, P., Dee, D., Fielding, K., Fuentes, M., Kallberg, P., Kobayashi, S., & Uppala, S. (2009). *The ERA-Interim Archive (ERA Report Series)*, *ERA report series*, (). Shinfield Park, Reading: European Centre for Medium-Range Weather Forecasts. Retrieved from. http://centaur.reading.ac.uk/1997/

Bourassa, M. A., Romero, R., Smith, S. R., & O'Brien, J. J. (2005). A new FSU winds climatology. *Journal of Climate*, *18*(17), 3686–3698. https://doi.org/10.1175/JCLI3487.1

Chang, K.-I., Ghil, M., Ide, K., & Lai, C.-C. A. (2001). Transition to aperiodic variability in a wind-driven double-gyre circulation model. *Journal of Physical Oceanography*, *31*(5), 1260–1286. https://doi.org/10.1175/1520-0485(2001)031<1260:TTAVIA>2.0.CO;2

Chen, Z., & Wu, L. (2011). Dynamics of the seasonal variation of the North Equatorial Current bifurcation. *Journal of Geophysical Research*, *116*, C02018. https://doi.org/10.1029/2010JC006664

Chen, Z., & Wu, L. (2015). Seasonal variation of the Pacific South Equatorial Current bifurcation. *Journal of Physical Oceanography*, *45*(6), 1757–1770. https://doi.org/10.1175/JPO-D-14-0085.1

Chen, Z., Wu, L., Qiu, B., Sun, S., & Jia, F. (2014). Seasonal variation of the South Equatorial Current bifurcation off Madagascar. *Journal of Physical Oceanography*, *44*(2), 618–631. https://doi.org/10.1175/JPO-D-13-0147.1

Chiang, T.-L., & Qu, T. (2013). Subthermocline eddies in the western equatorial Pacific as shown by an eddy-resolving OGCM*. *Journal of Physical Oceanography*, *43*(7), 1241–1253. https://doi.org/10.1175/JPO-D-12-0187.1

Hu, D., & Cui, M. (1989). *The western boundary current in the far western Pacific Ocean, (January 1989)* (pp. 123–134). Noumeéa: Inst. Fr. de Rech. Sci. pour le Deév. en Coop.

Hu, D., Hu, S., Wu, L., Li, L., Zhang, L., Diao, X., et al. (2013). Direct measurements of the Luzon undercurrent. *Journal of Physical Oceanography*, *43*(7), 1417–1425. https://doi.org/10.1175/JPO-D-12-0165.1

Jensen, T. G. (1991). Modeling the seasonal undercurrents in the Somali Current system. *Journal of Geophysical Research*, *96*(C12), 22,151. https://doi.org/10.1029/91JC02383

Jensen, T. G. (1993). Equatorial variability and resonance in a wind-driven Indian Ocean model. *Journal of Geophysical Research*, *98*(C12), 22,533. https://doi.org/10.1029/93JC02565

Jensen, T. G. (2001). Application of the GWR method to the tropical Indian Ocean*. *Monthly Weather Review*, *129*(3), 470–485. https://doi.org/10.1175/1520-0493(2001)129<0470:AOTGMT>2.0.CO;2

Jensen, T. G. (2003). Barotropic mode errors in an Indian Ocean model associated with the GWR method. *Global and Planetary Change*, *37*(1–2), 1–18. https://doi.org/10.1016/S0921-8181(02)00188-1

Jensen, T. G. (2011). Bifurcation of the Pacific North Equatorial Current in a wind-driven model: Response to climatological winds. *Ocean Dynamics*, *61*(9), 1329–1344. https://doi.org/10.1007/s10236-011-0427-2

Kalnay, E., Kanamitsu, M., Kistler, R., Collins, W., Deaven, D., Gandin, L., et al. (1996). The NCEP/NCAR 40-year reanalysis project. *Bulletin of the American Meteorological Society*, *77*(3), 437–471. https://doi.org/10.1175/1520-0477(1996)077<0437:TNYRP>2.0.CO;2

Kim, Y. Y., Qu, T., Jensen, T., Miyama, T., Mitsudera, H., Kang, H.-W., & Ishida, A. (2004). Seasonal and interannual variations of the North Equatorial Current bifurcation in a high-resolution OGCM. *Journal of Geophysical Research*, *109*, C03040. https://doi.org/10.1029/2003JC002013

Locarnini, R. A., Mishonov, A. V., Antonov, J. I., Boyer, T. P., Garcia, H. E., Baranova, O. K., et al. (2013). In S. Levitus (Ed.), A. Mishonov, Technical Ed.*World ocean atlas 2013. Volume 1, Temperature*, NOAA Atlas NESDIS 73, 40 pp. Silver Spring, Maryland: NOAA. https://doi.org/10.7289/V55X26VD

Matsuno, T. (1966). Numerical integrations of the primitive equations by a simulated backward difference method. *Journal of the Meteorological Society of Japan. Ser. II*, *44*(1), 76–84. https://doi.org/10.2151/jmsj1965.44.1_76

McCreary, J. P., & Kundu, P. K. (1988). A numerical investigation of the Somali Current during the Southwest Monsoon. *Journal of Marine Research*, *46*(1), 25–58. https://doi.org/10.1357/002224088785113711

McCreary, J. P., & Kundu, P. K. (1989). A numerical investigation of sea surface temperature variability in the Arabian Sea. *Journal of Geophysical Research*, *94*(C11), 16,097. https://doi.org/10.1029/JC094iC11p16097

McCreary, J. P., Miyama, T., Furue, R., Jensen, T., Kang, H.-W., Bang, B., & Qu, T. (2007). Interactions between the Indonesian throughflow and circulations in the Indian and Pacific Oceans. *Progress in Oceanography*, *75*(1), 70–114. https://doi.org/10.1016/j.pocean.2007.05.004

Menemenlis, D., Campin, J.-M., Heimbach, P., Hill, C., Lee, T., Nguyen, A., et al. (2008). ECCO2: High resolution global ocean and sea ice data synthesis. *Mercator Ocean Quarterly Newsletter*, Mercator Ocean Quarterly Newsletter. http://adsabs.harvard.edu/abs/2008AGUFMOS31C1292M

Nitani, H. (1972). Beginning of the Kuroshio. Kuroshio-Its Physical Aspects, 217–234. Retrieved from http://ci.nii.ac.jp/naid/10011288236/en/

Qiu, B., & Chen, S. (2010). Interannual variability of the North Pacific Subtropical Countercurrent and its associated mesoscale eddy field. *Journal of Physical Oceanography*, *40*(1), 213–225. https://doi.org/10.1175/2009JPO4285.1

Qiu, B., & Chen, S. (2012). Multidecadal sea level and gyre circulation variability in the northwestern tropical Pacific Ocean. *Journal of Physical Oceanography*, *42*(1), 193–206. https://doi.org/10.1175/JPO-D-11-061.1

Qiu, B., & Lukas, R. (1996). Seasonal and interannual variability of the North Equatorial Current, the Mindanao Current, and the Kuroshio along the Pacific western boundary. *Journal of Geophysical Research*, *101*(C5), 12,315–12,330. https://doi.org/10.1029/95JC03204

Qu, T. (2002). Depth distribution of the subtropical gyre in the North Pacific. *Journal of Oceanography*, *58*(3), 525–529. https://doi.org/10.1023/a:1021221500837

Qu, T., & Lukas, R. (2003). The bifurcation of the North Equatorial Current in the Pacific*. *Journal of Physical Oceanography*, *33*(1), 5–18. https://doi.org/10.1175/1520-0485(2003)033<0005:TBOTNE>2.0.CO;2

Qu, T., Mitsudera, H., & Yamagata, T. (1998). On the western boundary currents in the Philippine Sea. *Journal of Geophysical Research*, *103*(C4), 7537–7548. https://doi.org/10.1029/98JC00263

Reid, J. L., & Arthur, R. S. (1975). Interpretation of maps of geopotential anomaly for Deep Pacific Ocean. *Journal of Marine Research*, *33*, 37–52.

Rio, M. H., Guinehut, S., & Larnicol, G. (2011). New CNES-CLS09 global mean dynamic topography computed from the combination of GRACE data, altimetry, and in situ measurements. *Journal of Geophysical Research*, *116*, C07018. https://doi.org/10.1029/2010JC006505

Rodrigues, R. R., Rothstein, L. M., & Wimbush, M. (2007). Seasonal variability of the South Equatorial Current bifurcation in the Atlantic Ocean: A Numerical Study. *Journal of Physical Oceanography*, *37*(1), 16–30. https://doi.org/10.1175/JPO2983.1

Stommel, H., & Schott, F. (1977). The beta spiral and the determination of the absolute velocity field from hydrographic station data. *Deep Sea Research*, *24*(3), 325–329. https://doi.org/10.1016/0146-6291(77)93000-4

Sun, S., Wu, L., & Qiu, B. (2013). Response of the inertial recirculation to intensified stratification in a two-layer quasigeostrophic ocean circulation model. *Journal of Physical Oceanography*, *43*(7), 1254–1269. https://doi.org/10.1175/JPO-D-12-0111.1

Sverdrup, H. U. (1947). Wind-driven currents in a Baroclinic Ocean; with application to the equatorial currents of the Eastern Pacific. *Proceedings of the National Academy of Sciences*, *33*(11), 318–326. https://doi.org/10.1073/pnas.33.11.318

Toole, J. M., Millard, R. C., Wang, Z., & Pu, S. (1990). Observations of the Pacific North Equatorial Current bifurcation at the Philippine coast. *Journal of Physical Oceanography*, *20*(2), 307–318. https://doi.org/10.1175/1520-0485(1990)020<0307:OOTPNE>2.0.CO;2

Wang, Q., & Hu, D. (2006). Bifurcation of the north equatorial current derived from altimetry in the Pacific Ocean. *Journal of Hydrodynamics*, *18*(5), 620–626. https://doi.org/10.1016/S1001-6058(06)60144-3

Wang, Q., & Hu, D. (2012). Origin of the Luzon Undercurrent. *Bulletin of Marine Science*, *88*(1), 51–60. https://doi.org/10.5343/bms.2011.1020

Welander, P. (1968). Wind-driven circulation in one- and two-layer oceans of variable depth. *Tellus*, *20*(1), 1–16. https://doi.org/10.1111/j.2153-3490.1968.tb00347.x

Yang, J. (2015). Local and remote wind stress forcing of the seasonal variability of the Atlantic Meridional Overturning Circulation (AMOC) transport at 26.5 °N. *Journal of Geophysical Research: Oceans*, *120*, 2488–2503. https://doi.org/10.1002/2014JC010317

Zhang, L., Hu, D., Hu, S., Wang, F., Wang, F., & Yuan, D. (2014). Mindanao Current/Undercurrent measured by a subsurface mooring. *Journal of Geophysical Research: Oceans*, *119*, 3617–3628. https://doi.org/10.1002/2013JC009693

Zuo, H., Balmaseda, M. A., & Mogensen, K. (2017). The new eddy-permitting ORAP5 ocean reanalysis: Description, evaluation and uncertainties in climate signals. *Climate Dynamics*, *49*(3), 791–811. https://doi.org/10.1007/s00382-015-2675-1

Zweng, M. M., Reagan, J. R., Antonov, J. I., Locarnini, R. A., Mishonov, A. V., Boyer, T. P., et al. (2013). In S. Levitus (Ed.), A. Mishonov, Technical Ed*World ocean atlas 2013. Volume 2, Salinity*, NOAA Atlas NESDIS 74, (). Silver Spring, Maryland: NOAA. 39 pp